# Electronic structure of Mg-Zn-based compounds

Yasushi Ishii, Zoltan Dankhazi, Esther Belin-Ferré


# Electronic structure of Mg-Zn-based compounds

| | |
|---|---|
| Journal: | *Philosophical Magazine & Philosophical Magazine Letters* |
| Manuscript ID: | TPHM-10-May-0210.R1 |
| Journal Selection: | Philosophical Magazine |
| Date Submitted by the Author: | 21-Sep-2010 |
| Complete List of Authors: | Ishii, Yasushi; Chuo University, Department of Physics<br>Dankhazi, Zoltan; Eötvös Loránd University, Department of Materials Physics,<br>Belin-Ferré, Esther; Laboratoire de Chimie Physique Matièrev et Rayonnement UMR 7614 |
| Keywords: | band calculations, electronic density of states, electronic structure |
| Keywords (user supplied): | |
| | |

# Electronic structure of Mg-Zn-based compounds

Yasushi Ishii,[1] Zoltan Dankhazi[2] and Esther Belin-Ferré[3*]

1 -Department of Physics, Chuo University, Kasuga, Bunkyo-ku, Tokyo 112-8551, Japan.
2-Department of Materials Physics, Eötvös Loránd University Budapest
1117 Budapest, Pázmány P. stny. 1/A, Hungary
3- Laboratoire de Chimie Physique-Matière et Rayonnement, Unité Mixte de Recherche CNRS-UPMC 7614
11 rue Pierre et Marie Curie, 75231 Paris cedex 05, France

*Corresponding author : esther.belin-ferre@upmc.fr*

**Abstract.** We present a comparison between calculated densities of states of the Laves phase $MgZn_2$ and hexagonal $Mg_{28}Zn_{65}Y_7$ and experimental results obtained using both X-ray emission and photoabsorption spectroscopy techniques. We show that there is a general agreement between both sets of data for both alloys. We also point out the two samples retain a metallic character yet, the hexagonal approximant of the Mg-Zn-Y quasicrystals family is less metallic than the Laves phase.

## 1. Introduction

Experimental investigation of the electronic structure of complex compounds is nowadays supported by the densities of states (DOS) calculated by using various first-principles techniques such as the tight-binding linear-muffin-tin-orbital (TB-LMTO) method[1] or the pseudopotential method which is used, for example, in the Vienna *ab initio* simulation package (VASP)[2] ; such calculations are also made possible thanks to accurate determination of the atomic structures by x-ray or (and) electron diffraction experiments.

We report here on a comparison between calculated and experimental DOS for the Laves phase $MgZn_2$ and hexagonal $Mg_{28}Zn_{65}Y_7$ which is an approximant of the family of Mg-Zn-Y quasicrystals.

In the next section of this paper we introduce some information about the atomic structure of the two specimens. Section 3 is dedicated to experimental procedures, and section 4 reports the DOS calculations. Section 5 is dedicated to the comparison between calculation and experiment and finally, we give a short conclusion in section 6.

## 2. Atomic structure of $MgZn_2$ and $Mg_{28}Zn_{65}Y_7$

Mg-Zn-RE (RE=Y or rare-earth elements) alloys form a series of unique hexagonal crystals in a composition range close to that of icosahedral quasicrystals of the same system, with almost the same periodicity along the c-axis, namely $c$ = 8.6 Å. The space group of the hexagonal phases is $P6_3/mmc$ and the lattice parameters are reported to be $a$ = 14.6, 23.5 and 33.6 Å.[3] It is interesting to note that the periodicities in the hexagonal plane are scaled approximately according to the golden mean. The hexagonal Laves (C14) phase, $MgZn_2$, which is a typical Frank-Kasper alloy with the tetrahedrally closed-packed structure and unit cell parameters $a$ = 5.2Å and $c$ = 8.6 Å may be involved in this family.[4]

We investigate here the hexagonal phase with the smallest lattice parameter i.e. $a$ = 14.6 Å and the hexagonal Laves phase. The crystal structure of the hexagonal phase has been studied by Takakura *et al.*[5] In this phase, there is one fractional site occupied by either Mg or Y with probability 0.85 for Mg occupancy. In the electronic structure calculations presented below, we assume that this fractional site is fully occupied by Mg. Hence the composition of the model hexagonal structure is $Mg_{26}Zn_{60}Y_6$ ($Mg_{28}Zn_{65}Y_7$ in atomic %).

## 3. Experimentals

Soft X-ray Emission and Soft X-ray Absorption Spectroscopies, denoted hereafter as SXES and SXAS, respectively, allow investigating DOS of a bulk solid, whether it is crystalline, amorphous,

metallic, insulator, etc. SXES scans the radiative recombination of a core hole from an outer level or the valence band whereas in SXAS, radiation is absorbed to promote an inner electron to an originally empty level (for more details see for example reference 6). The X-ray transitions are governed by dipole selection rules ($\Delta\ell = \pm 1$ and $\Delta j = 0, \pm 1$) so that SXES and SXAS techniques are characterised by a double spectral and chemical selectivity and accordingly, SEXS probes separately *s, p, d*... occupied states around each chemical species of the solid whereas SXAS probes the unoccupied counterparts. The transition probabilities are constant or vary slowly within the energy range of a valence band (VB) or the first eV's of a conduction band (CB) therefore, the intensity of the emitted (alternatively absorbed) radiation is proportional to the convolution product of the probed occupied $N_{occupied}$ (alternatively unoccupied $N_{unoccupied}$) DOS by the lorentzian energy distribution associated to the life time of the inner hole involved in the X-ray transition, hence:

$$I_{(emitted)} \propto N_{(occupied)} * \mathcal{L}_{(inner\ level)} \quad \text{and} \quad I_{(absorbed)} \propto N_{(unoccupied)} * \mathcal{L}_{(inner\ level)}$$

Note that whereas *p* states are probed alone, *s* and *d* states are obtained together. However, the transition probabilities favour *d* states with respect to *s* ones. The energy resolution of the technique is driven by $\mathcal{L}$ which varies from 0.01 eV to a few eV according to the element and the inner level under consideration.[7]

Although these techniques do not provide absolute DOS values, it makes sense to compare same spectral distributions of a given element in various compounds since changes in the shapes of the spectral distributions go along with changes in electronic interactions. The spectral curves are obtained each one in its own X-ray transition energy scale. A description of the VB and CB bands, is achieved provided the various spectra are adjusted on a same energy scale. It is convenient to use the binding energy scale which allows for direct comparison between the experimental data and occupied and unoccupied partial DOS calculations. For such a purpose, we place $E_F$ on each X-ray transition energy scale principally owing to complementary measurements of inner levels binding energies.[8]

The x-ray transitions studied here are listed in Table 1. The SXES experiments were carried out in vacuum spectrometers fitted with either a crystal slab or a grating. The SXAS spectra were obtained at the synchrotron facility (LURE, Orsay, France) with two crystal spectrometers. The energy resolutions were about 0.4, 0.7 and 2 eV for Mg, Zn and Y, respectively.

Table 1. Experimental energy ranges for the various investigated X-ray transitions

| X-ray transition | Probed states | Monochromator | Energy range (eV) |
|---|---|---|---|
| Mg Kβ | VB→ 1s | beryl 10 $\bar{1}$ 0 | 1275-1305 |
| Mg $L_{2,3}$ | VB→ $2p_{1/2,3/2}$ | grating (600 groves/mm) | 35-55 |
| MgK | CB← 1s | beryl 10 $\bar{1}$ 0 | 1300-1335 |
| Y $L_3$ | CB← $2p_{3/2}$ | Ge 111 | 2065-2095 |
| Zn $L_3$ | CB← $2p_{3/2}$ | beryl 10 $\bar{1}$ 0 | 1294-1335 |

Because of the low concentration of Y in the hexagonal specimen (7%) which raises low background/signal ratio, we did not investigate Y occupied states but the high flux of the incident photon line at LURE, allowed us to obtain the corresponding CB states.

## 4. Calculations

DOS calculations have been done with the tight-binding linear muffin-tin orbitals method (TB-LMTO) in the atomic-sphere approximation (ASA).[1] Non-atomic Mg-*d* states are explicitly considered to improve description of *d-like* states near the Fermi energy. Electron-electron interaction is treated within the local-density approximation (LDA) in the density-functional theory.[9] The Brillouin-zone integration is done by a conventional tetrahedron method with the k-point meshes of 20x20x12 (308 irreducible k-points) and 8x8x12 (70 irreducible k-points) for the $Zn_2Mg$ Laves and the Zn-Mg-Y hexagonal phases, respectively. Here the k-point meshes are taken to realize similarly fine sampling of the Brillouin-zone for different lattice parameters.

The total DOS is shown in Fig.1 together with partial DOS for *s*-, *p*- and *d*- partial waves, with the Fermi energy $E_F$ taken as zero. The peak at around 8eV below $E_F$, comes from the Zn-3*d* band and does not contribute significantly to the stabilization of these systems. One can see a deep minimum of the DOS (pseudogap) near the Fermi energy for the hexagonal $Mg_{28}Zn_{65}Y_7$ but it is not clearly seen for the hexagonal Laves phase. Enhancements of the *p*-DOS below $E_F$ and the *d*-DOS above $E_F$ suggest that the *p*-*d* hybridization is important for the pseudogap formation. Note here that the *d*-DOS above $E_F$ mainly comes from the Y-4*d* states, which is missing for the Laves case.[10,11]

In the following section, we shall show partial components of the calculated DOS separately to make direct comparison with the SXES and SXAS results.

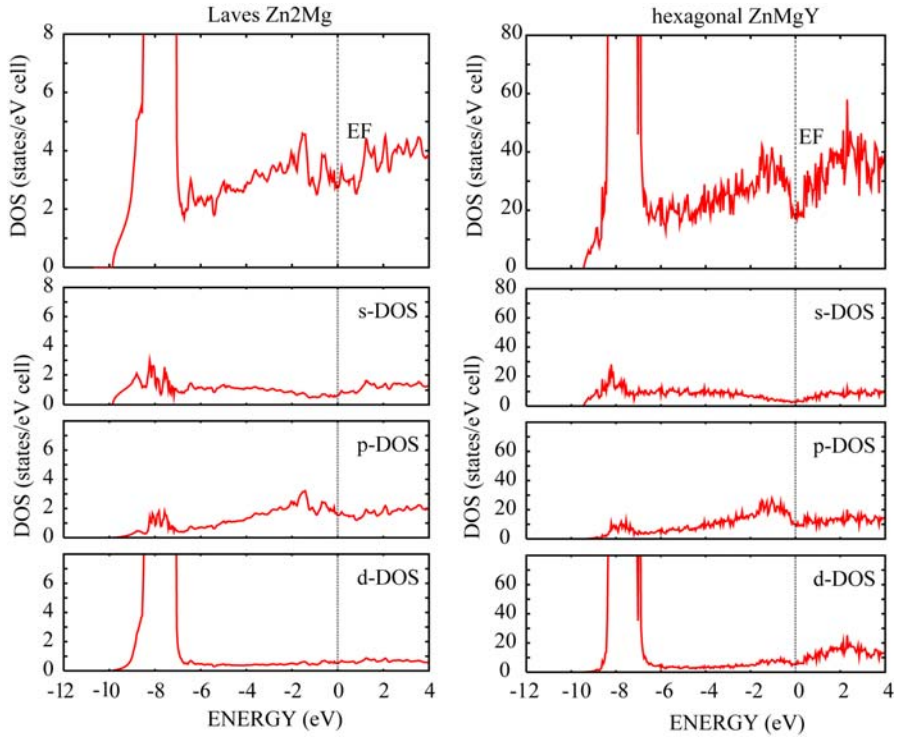


Fig.1 : Total electronic density of states for the hexagonal Laves $MgZn_2$ (left) and the hexagonal $Mg_{28}Zn_{65}Y_7$ (right) together with the corresponding *s*- *p*- and *d*-partial DOS (lower panels).

## 5. Results

### a) Calculations

For meaningful comparison with the experimental results all partial calculated distributions have been broadened by a Lorentzian distribution $\mathcal{L}$ to account for the life time of the core hole involved in the studied x-ray transition and a Gaussian distribution G to account for the instrumental function of the spectrometers (Table 2). Also, for direct comparison to experimental data, the theoretical curves are normalized to give the same maxima for different components. The absolute intensity of the Mg-*d* DOS, for example, is very small in comparison with the other components

.

Table 2. Energy broadenings applied to the calculated partial DOS.

| Investigated states | L (eV) | G (eV) |
|---|---|---|
| Mg p | 0.36 | 0.4 |
| Mg s,d | 0.1 | 0.4 |
| Zn s,d | 0.65 | 0.4 |
| Y s,d | 1.5 | 0.4 |

The resulting so-called "theoretical curves" are plotted in Figures 2-a and 2-b for the Laves phase and in Figures 2-c and 2-d for the hexagonal compound. Note that unoccupied DOS are shown over about 8 eV only because beyond such an energy extent the calculated DOS are less accurate and meaningful than the DOS calculated for the occupied counterparts.

The valence band of the $MgZn_2$ Laves phase (Fig. 2-a) displays first Mg *d* states at $E_F$- 0.92 eV, followed by Mg *p* states at $E_F$-1.72 eV then a broad band of Mg *s* states whose maximum is at $E_F$-3.44 eV, a narrow band of Zn *d* states is present at 7.69 eV from $E_F$. This band overlaps with peaks of the Mg partial distributions suggesting Zn-Mg hybridization in this energy range of the valence band. The peaks in the Mg DOS are enhanced because of the high DOS for the Zn 3*d* bands. The wave functions for the Zn 3d bands consist mainly of the Zn 3d states with small amount of the Mg 3s, 3p, d components hence smaller probabilities for the X-ray transition associated with Mg. Note that (i) Zn *s* states are not shown because the experiment cannot account for them due to transition probabilities and (ii) the contribution of Zn *d* states in the vicinity of $E_F$ is vanishing.

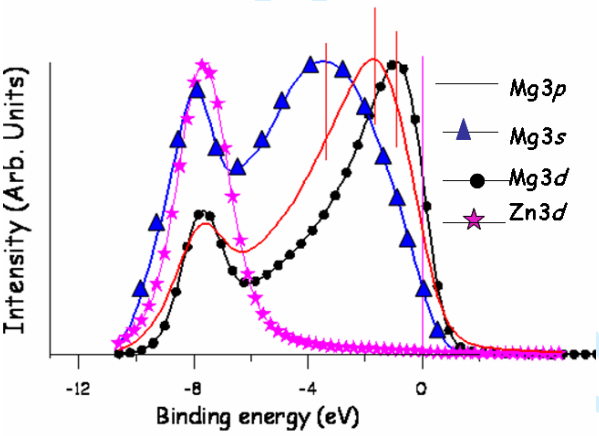


Fig. 2-a: Valence band of $MgZn_2$. The respective maxima are shown by vertical bars.

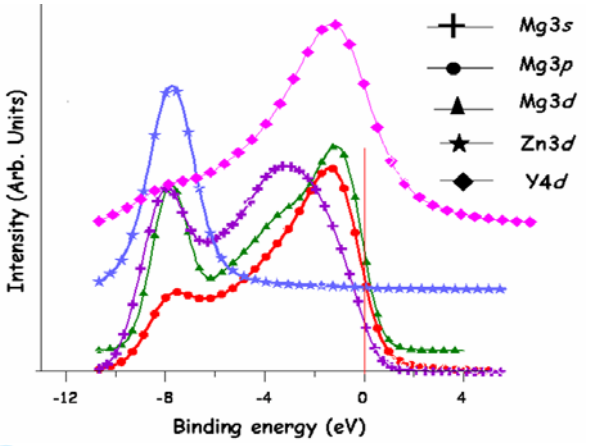


Fig. 2-c: Valence band of hexagonal $Mg_{28}Zn_{65}Y_7$For clarity, the curves are shifted along the y-axis.

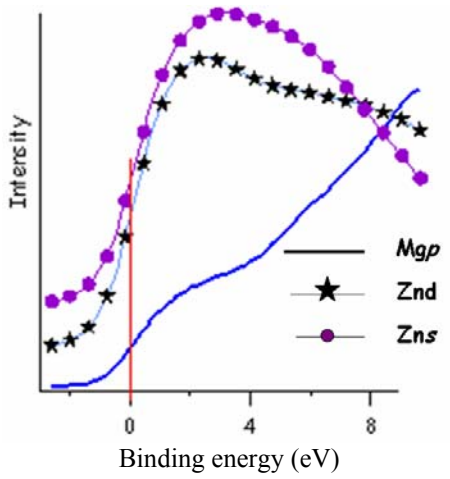


Fig. 2-b: Conduction band of $MgZn_2$. For clarity, the spectral curves are shifted along the y-axis.

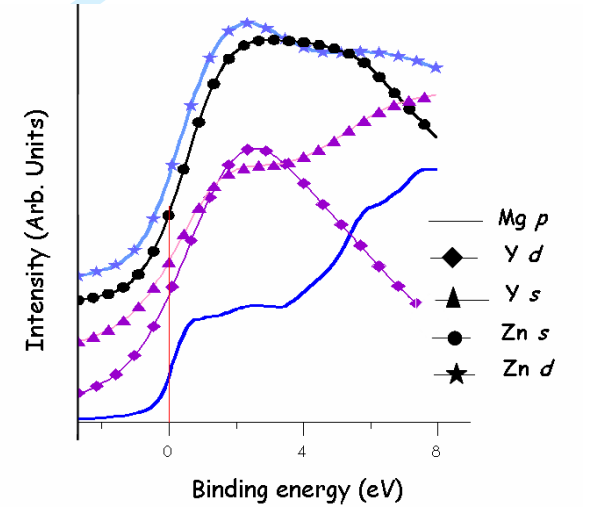


Fig. 2-d: Conduction band of hexagonal $Mg_{28}Zn_{65}Y_7$. For clarity, the spectral curves are shifted along the y-axis.

In hexagonal $Mg_{28}Zn_{65}Y_7$, the valence band (Fig. 2-c) shows Mg *d* states at $E_F$-1.15 eV immediately followed by Y *d* states at $E_F$-1.26 eV, then Mg *p* states at $E_F$-1.37, Mg *s* and Y *s* states are at $E_F$-3.17 eV and $E_F$-3.61 eV, respectively and finally Zn *d* and Zn *s* states are found at $E_F$-7.77 eV and $E_F$-7.99 eV respectively. Therefore there is significant interaction between Mg *p*, Mg *d* and Y *d* states at the top of the valence band, between Mg *s* and Y *s* states in the middle of the band whereas all

Zn states lie far from $E_F$, at the bottom of the band. The conclusions reported above for Zn *d* spectral distribution near $E_F$ hold true for hexagonal $Mg_{28}Zn_{65}Y_7$ as well.

As far as the conduction bands are concerned, Figs 2-b and 2-d show that all partial distributions totally overlap indicating thus a total mixing of the states at the bottom of the conduction band. For both compounds the maximum of the bump of Zn *d* states curves coincide with changes of slope of the Mg *p* ones. For the hexagonal compound, the maximum of the Y *d* distribution curve is set at about half length of the Mg *p* states plateau and coincides with the respective maxima of the Mg *d* and Zn *d* curves thus pointing out strong mixing of all *d* states.

**b) Experiments**

***1- $MgZn_2$ Laves phase***

Left panel of Fig. 3 shows the valence band for the Laves phase where the experimental Mg 3*s*,*d*, Mg 3*p* and Zn 3*d*-4*s* partial distributions have been adjusted to the binding energy scale. This was achieved as mentioned above, thanks to the determination of the binding energies of the inner levels involved in the X-ray transitions by using photoemission spectroscopy measurements.

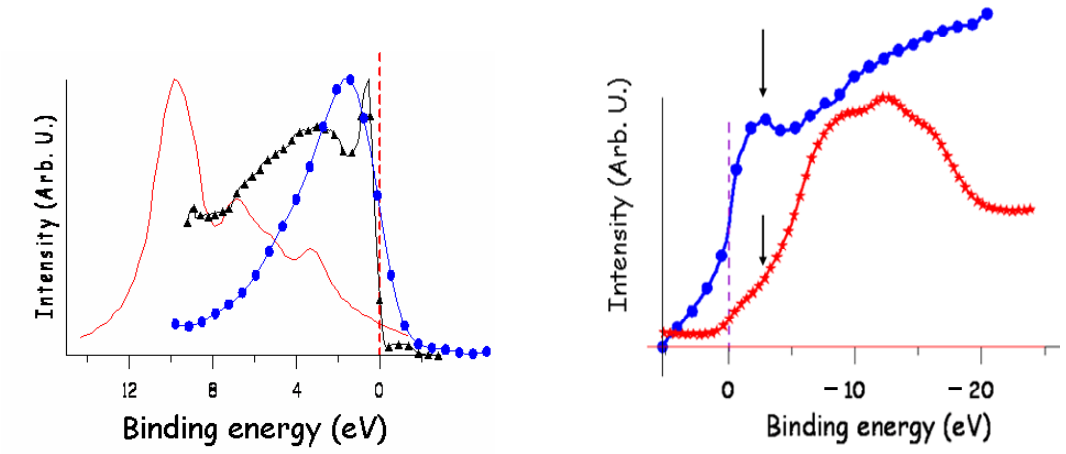


Fig. 3. Left panel: Valence band of the Laves phase, the Mg 3*s*,*d* (curve with triangles), Mg 3*p* (curve with solid circles) and Zn 3*d*-4*s* (curve without symbols) distributions in $Zn_2Mg$, adjusted to the binding energy scale. The features seen on the Zn 3*d*-4*s* curve towards $E_F$ are satellites of the main line and do not refer to features of the genuine DOS. Right panel: conduction band: partial Zn *d* (curve with solid circles) and Mg *p* (curve with stars) distributions are also adjusted to the binding energy scale. The arrows show the maximum of the Zn *d* peak coincides with the shoulder of the Mg *p* states distributions, in agreement with the calculated curves (see text).

The general features of the calculated valence band are accounted for by the experiment except for the one at about 8 eV from $E_F$ which is observed neither on the experimental Mg 3*p* states distribution nor the Mg 3*s*,*d* one. The experimental Zn 3*d*-4*s* component shows a peak at about 10 eV below $E_F$ whereas the calculated Zn *d* band appears at 7-8 eV below $E_F$. This is due to the exchange-correlation energy functional in the LDA that induces a well-known self-interaction error.[12]

The narrow peak close to $E_F$ in the Mg 3*s*,*d* curve is reminiscent of a similar even much more narrow peak present in the experimental 3*s*,*d* distribution for pure Mg. This peak in the metal is in part ascribed to a many body effect following the creation of the inner hole in the free electron metal.[13] Therefore, here, the presence of this narrow peak suggests the Laves phase retains a marked metallic behaviour. Except for the feature at $E_F$ - 8 eV, the shape of the Mg 3*p* distribution agrees with the calculation and the maximum of the distribution is at 1.7 ± 0.1 eV and also matches with the calculation. Within the experimental precision, the intensity at $E_F$ is about 50% the total intensity. This also gives indication that the compound retains a metallic character as was already pointed out in reference 14 for Al-based alloys and compounds. The maximum of the Mg 3*s*,*d* distribution is at 0.3 ± 0.1 eV and a bump is noticeable at 3. 0 ± 0.2 eV. This is again rather consistent with the calculated

results. The curve for Zn 3*d*-4*s* states reflects mainly the contribution due to *d* states because, as mentioned above, x-ray transition probabilities noticeably favour *d* states with respect to *s* ones, therefore in elements where the *d* sub-band is filled or almost filled, 4*s* states are not observed. The maximum of the distribution is found far from $E_F$, hence we verify experimentally that Zn states do not contribute at the edge of the valence band. As explained above, the two features located around 7 eV and 3 eV are satellites formed during the x-ray process.

The right panel of Fig. 3 presents the Zn *d* and Mg *p* contributions to the conduction band adjusted to the binding energy scale similarly to distributions of the valence band. Their shapes and energy positions agree with the calculated curves although some inaccuracy may be involved in the Zn spectral distributions due to the faint contribution to $E_F$ as underlined above. Due to experimental constraints the other partial contributions to the conduction band could not be measured, however, from the present data, we conclude the experimental results for the Laves phase are consistent with the theoretical calculations.

### *2- Hexagonal compound $Mg_{28}Zn_{65}Y_7$*

For this compound we measured the Mg 3*p* and Mg3*s*,*d* states. We verified that Zn 3*d*,4*s* states are set very far from $E_F$ and because of the low concentration, we did not measure Y states. The corresponding curves are shown in the left panel of Fig. 4.

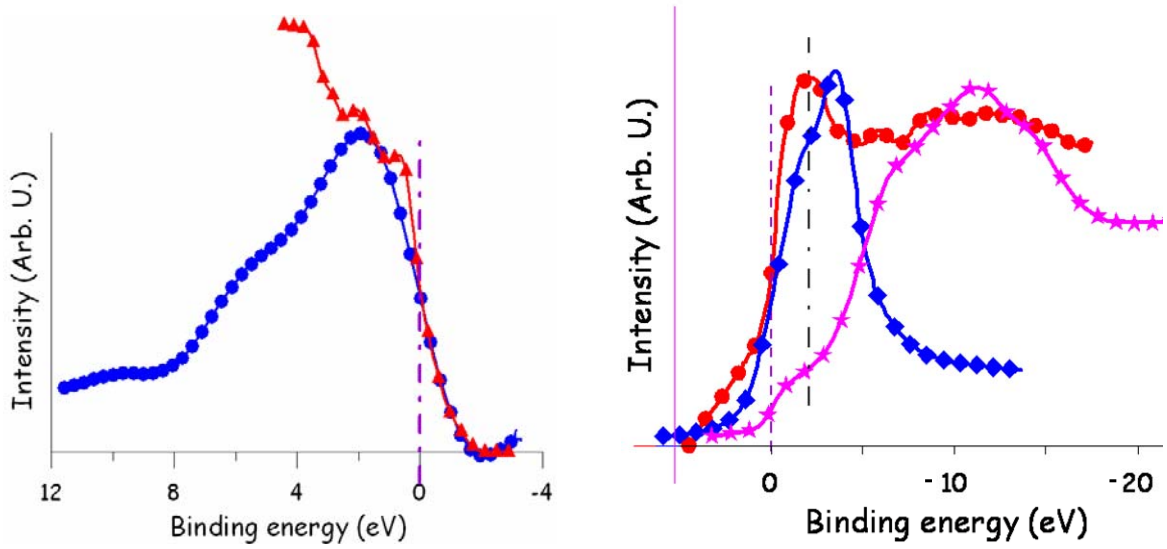


Figure 4: Left panel: Valence band of the hexagonal phase. the Mg 3*s*,*d* (curve with triangles), Mg 3*p* (curve with solid circles) distributions adjusted to the binding energy scale. Right panel: partial Zn *d* (curve with solid circles), Mg *p* (curve with stars) and Y*s*,*d* (curve with diamonds) conduction band distributions. The dash-dot vertical line points out the coincidence between the Zn *d* peak and the shoulder of the Y *s*,*d* curve (see text).

The Mg 3*s*,*d* states distribution is plotted only over a few eV below $E_F$ because one intense Y atomic line of the compound is excited during the Mg 3*s*,*d* x-ray emission process and lies at about 7 eV below $E_F$. The contribution of this line to the spectrum could not be removed exactly. However, this Lorentzian-like line is narrow enough for its contribution to the spectrum in the energy range plotted here, 2 eV below $E_F$, to be neglected so that the features of the part of the Mg 3*s*,*d* curve shown on the figure actually is meaningful. In particular we note the abrupt edge is consistent with the calculation. The peak of this curve above the edge is at $E_F$ - 0.7 ± 0.1 eV whereas in the calculation the Mg *d*-like peak is present at 1.15 eV below $E_F$. All the same there is a discrepancy as far as Mg 3*p* distribution is concerned since the experiment finds its maximum at $E_F$ - 1.9 ± 0.1 eV against -1.37 eV below $E_F$ in the calculation. However, we note that the Mg 3*s*,*d* states are found closer to $E_F$ than the Mg 3*p* states. By analogy to Al based compounds, because of the strong similarities that exist between Al and Mg states distributions,[15] we may reasonably assume that the first states below the Fermi

energy are of Mg with a *d*-like character. Therefore, there is consistency between the experiment and the calculations since these latter suggest a larger contribution of the Mg-*d* states near the Fermi energy than the Mg *p* states and hence the Mg-*d* peak in the calculation shifts towards $E_F$. The narrow peak at the Fermi energy of the Mg 3*s*,*d* spectrum we observed in the Laves phase is not clearly seen for the hexagonal compound. We already mentioned that such a peak is present in free-electron metals like fcc Al and hcp Mg. Since it is almost absent here, we can conclude that the hexagonal approximant should be slightly less metallic than the simple intermetallic compound $MgZn_2$. A direct comparison with experimental data for the electric resistivity of the same samples would have been of interest here but could not been achieved because of a lack of results available for both compounds for the time being.

The curve corresponding to the Mg 3*p* states displays a smooth bump around 6 eV below $E_F$ that is not expected from the calculation. This bump may be due to remaining participation to the spectrum of oxide contribution in this energy range that is difficult to remove totally with accuracy from the experimental data in Mg alloys and compounds. Here the sample was somewhat oxidized although no significant oxide contribution could be detected in the Mg unoccupied counterpart. However, from our previous investigations of pure Mg, we know that there is no oxide contribution in the energy range that involves 2 eV below $E_F$ which is actually the energy range of main interest here. Within the experimental accuracy, the intensity of the Mg 3*p* distribution at $E_F$ is almost 50% of the total intensity in our sample whereas in hcp Mg it is 50% of the total intensity, as expected for a free-electron metal. The slight decrease in the intensity of the 3p states of the hexagonal compound suggests a very shallow pseudo-gap forms in the conducting states arising from Mg and accordingly the specimen should be not as metallic as the pure metal, consistently with our conclusions from the study of the Mg 3*s*,*d* spectrum of the same hexagonal specimen.

The right panel of Fig. 4 shows the Zn *s*-*d*, Mg *p* and Y *s*-*d* contributions to the conduction band of the hexagonal compound. The shape of the experimental Mg *p* curve is consistent with the calculation. We observe a marked peak above the steep edge of the Zn *s*-*d* and Y *s*-*d* experimental curves consistently with the calculation despite the low Zn intensity at $E_F$. The coincidence between the maximum of the Zn *s*-*d* curve and a shoulder just above $E_F$ of the Y *s*,*d* one points out strong interaction, namely covalency, between these states in this energy range. According to the calculation (see figure 2d), the shoulder of the Y *s*,*d* curve should correspond to a contribution of states with *s* character whereas the main peak is due to *d* states. Remember that transition probabilities favour d states with respect to s ones. The principal part of both Zn and Y experimental *s*,*d* peaks is more marked than expected from the calculation. This suggests the states of the conduction band located near the Fermi level should retain a significant localized character.

## 4. Concluding remarks

We have measured several partial electronic distributions of the valence and conduction bands of the Laves phase $MgZn_2$ and hexagonal $Mg_{28}Zn_{65}Y_7$ by using X-ray emission and photoabsorption spectroscopy techniques. A general agreement has been found between the experimental results and DOS calculations for the two alloys. From the study of the valence band, we ascertained both samples retain a metallic character yet, the hexagonal approximant of the Mg-Zn-Y quasicrystals family is less metallic than the Laves phase. This is confirmed by the analysis of the conduction band of the hexagonal approximant that shows a tendency to localisation of the states nearby the Fermi level. This is consistent with conclusions for other families of quasicrystals and approximants, especially Al-transition metal based, where Al states close to $E_F$ are mixed to *d* states from the transition element which gives rise to the so called *sp*-*d* hybridisation, in part responsible for the formation of a pseudo-gap at $E_F$ in these compounds.[11,14,16,17]

**Acknowledgements**. Thanks are due to Pr. Anne Sadoc for measurements at LURE and to Dr. Herbert Mueller from Technical University, Vienna, (Austria) for hospitality and help during Mg 3s,d measurements. We also acknowledge Pr. An Pang Tsai, for providing well characterised samples. We are glad to point out how profitable have been discussions with Pr. Uichiro Mizutani, Dr. Jean Marie Dubois and Dr. Marc de Boissieu.

## References


1. O. K. Andersen, O. Jepsen, and D.Glötzel, *Highlight in Condensed Matter Theory,* edited by F. Bassani, F. Fumi, and M. P. Tosi (North-Holland, New York, 1985), p.59.
2. G. Kresse and J. Hafner, *Phys. Rev.* B **47** 558 (1993); G. Kresse and J. Furthmüller, *Phys. Rev.* B **54** 11169 (1996).
3. E.Abe, H.Takakura, A.Singh and A.P.Tsai, *J. Alloys Compounds*, **283** (1999), 169; K.Sugiyama, K.Yasuda, T.Ohsuna and K.Hiraga, *J. Alloys Compounds*, **285** 172(1999).
4. T.Ohba, Y.Kitano and Y.Komura, *Acta Crystallogr*. **C 40** 1(1984).
5. H.Takakura, A.Sato, A.Yamamoto and A.P.Tsai, *Phil. Mag. Lett*. **78** 263 (1998).
6. B.K. Agarwal, *X-Ray Spectroscopy* (Optical Series, S987, Springer Verlag, Berlin) 1979; C. Bonnelle, *Annual Report C, R. Soc. Chemistry of London* 201 *(*1987).
7. M. O. Krause and J. H. Oliver *J. Phys. Chem. Data* **8-2** 329 (1979).
8. E. Belin and A.Traverse , *J. of Physics : Cond. Matter* **3** 2157 (1991).
9. P. Hohenberg and W. Kohn, *Phys. Rev*. **136** B864 (1964) ; W.Kohn and L.J.Sham, *Phys. Rev.* **140** A1133 (1965).
10. K.Oshio and Y.Ishii, J. Alloys and Compounds **342** 402 (2002).
11. Y.Ishii and T.Fujiwara, *Quasicrystals*, edited by T.Fujiwara and Y.Ishii (Elsevier, 2007), p.171.
12. J. P. Perdew and A. Zunger, *Phys. Rev. B* **23** 5048 (1981).
13. P. Nozières and C.T. de Dominicis, *Phys. Rev.* **178** 6105 (1969).
14. E. Belin-Ferré, V. Fournée and J. M. Dubois, *Materials Transactions JIM*, **42** 911 (2001).
15. D. A. Papaconstantopoulos, *Handbook of the Band Structure of Elemental Solids* (Plenum Press, New York, 1986); private communication (2008).
16. U Mizutani, *CMA series, Vol.2.* (World Scientific, Singapore, to be published).
17. G. Trambly de Laissardière, D. Nguyen Manh, D. Mayou, Progress in Materials Science **50**, 679 (2005).


## Table captions

Table 1. Experimental energy ranges for the various investigated X-ray transitions

Table 2. Energy broadenings applied to the calculated partial DOS.

## Figure captions

Figure 1 : Total electronic density of states for the hexagonal Laves $MgZn_2$ (left) and the hexagonal $Mg_{28}Zn_{65}Y_7$ (right) together with the corresponding *s*- *p*- and *d*-partial DOS (lower panels).

Figure 2-a: Valence band of $MgZn_2$. The respective maxima are shown by vertical bars.

Figure 2-b: Conduction band of $MgZn_2$. For clarity, the spectral curves are shifted along the y-axis.

Figure 2-c: Valence band of hexagonal $Mg_{28}Zn_{65}Y_7$. For clarity, the spectral curves are shifted along the y-axis.

Fig. 2-d: Conduction band of hexagonal $Mg_{28}Zn_{65}Y_7$. For clarity, the spectral curves are shifted along the y-axis.

Figure 3: Left panel: Valence band of the Laves phase, the Mg 3*s,d* (curve with triangles), Mg 3*p* (curve with solid circles) and Zn 3*d*-4*s* (curve without symbols) distributions in $Zn_2Mg$, adjusted to the binding energy scale. The features seen on the Zn 3*d*-4*s* curve towards $E_F$ are satellites of the main line and do not refer to features of the genuine DOS. Right panel:

conduction band: partial Zn *d* (curve with solid circles) and Mg *p* (curve with stars) distributions are also adjusted to the binding energy scale. The arrows show the maximum of the Zn *d* peak coincides with the shoulder of the Mg *p* states distributions, in agreement with the calculated curves (see text).

Figure 4: Left panel: Valence band of the hexagonal phase. the Mg 3*s,d* (curve with triangles), Mg 3*p* (curve with solid circles) distributions adjusted to the binding energy scale. Right panel: partial Zn *d* (curve with solid circles), Mg *p* (curve with stars) and Y*s,d* (curve with diamonds) conduction band distributions. The dash-dot vertical line points out the coincidence between the Zn *d* peak and the shoulder of the Y *s,d* curve (see text).